THE JOURNAL OF BIOLOGICAL CHEMISTRY VOL. 286, NO. 10, pp. 8000–8013, March 11, 2011

Redesign of a Plugged β-Barrel Membrane Protein*[S]

Received for publication, October 25, 2010, and in revised form, December 16, 2010 Published, JBC Papers in Press, December 28, 2010, DOI 10.1074/jbc.M110.197723

Mohammad M. Mohammad[‡1], **Khalil R. Howard**[§1], **and Liviu Movileanu**[‡§¶2]

From the [‡]*Department of Physics, Syracuse University, Syracuse, New York 13244-1130, the* [§]*Structural Biology, Biochemistry, and Biophysics Program, Syracuse University, Syracuse, New York 13244-4100, and the* [¶]*Syracuse Biomaterials Institute, Syracuse University, Syracuse, New York 13244*

The redesign of biological nanopores is focused on bacterial outer membrane proteins and pore-forming toxins, because their robust β-barrel structure makes them the best choice for developing stochastic biosensing elements. Using membrane protein engineering and single-channel electrical recordings, we explored the ferric hydroxamate uptake component A (FhuA), a monomeric 22-stranded β-barrel protein from the outer membrane of *Escherichia coli*. FhuA has a luminal cross-section of 3.1 × 4.4 nm and is filled by a globular N-terminal cork domain. Various redesigned FhuA proteins were investigated, including single, double, and multiple deletions of the large extracellular loops and the cork domain. We identified four large extracellular loops that partially occlude the lumen when the cork domain is removed. The newly engineered protein, FhuAΔC/Δ4L, was the result of a removal of almost one-third of the total number of amino acids of the wild-type FhuA (WT-FhuA) protein. This extensive protein engineering encompassed the entire cork domain and four extracellular loops. Remarkably, FhuAΔC/Δ4L forms a functional open pore in planar lipid bilayers, with a measured unitary conductance of ~4.8 nanosiemens, which is much greater than the values recorded previously with other engineered FhuA protein channels. There are numerous advantages and prospects of using such an engineered outer membrane protein not only in fundamental studies of membrane protein folding and design, and the mechanisms of ion conductance and gating, but also in more applicative areas of stochastic single-molecule sensing of proteins and nucleic acids.

One critical prerequisite for developing a sensitive stochastic sensing element is a robust protein scaffold (1–3). Recent studies in structural biology have revealed that β-barrel membrane proteins fulfill such a requirement (4, 5). A β barrel folds into a roughly cylindrical pore with the hydrophilic side chains oriented inside the pore lumen and the hydrophobic residues exposed to the lipid bilayer. Because the network of backbone hydrogen bonds between the neighboring β strands imparts an extraordinary stiffness to the core of the protein, β barrels are open to remodeling in various ways, including direct genetic engineering and covalent modifications (1, 6, 7). Although redesigned β-barrel proteins are essential for stochastic biosensors, their broad application to this realm has been limited to the trimeric OmpF porins (8–10) and the heptameric α-hemolysin (αHL)[3] pore-forming toxin (Table 1) (1, 3, 11, 12). The multimeric character of these proteins makes them less than ideal for remodeling work (Table 1 and supplemental Fig. S1). For example, the stoichiometry and symmetry of the *homomeric* β-barrel pores generate many permutations and combinations of the modified (or engineered) and unmodified (wild type) monomers. This is the major reason for the technical difficulties of separating the engineered single subunit-modified protein pores with well defined biophysical and biochemical features from other products of the oligomerization reaction (13, 14).

Recently, the outer membrane protein G (OmpG), a monomeric β-barrel pore, whose single-channel conductance and inner diameter are comparable with the corresponding values of the αHL pore (~1 nS and ~15 Å, respectively) (15), was engineered to produce a quiet unitary conductance (16). Thus, the engineered OmpG protein might function as a nanopore-based biosensor for stochastic detection via noncovalent adaptors. However, the x-ray crystal structures of both αHL (4) and OmpG (15) proteins reveal a somewhat small diameter of the constriction region of the pore (~15 Å), allowing the translocation of small molecules up to ~700 Da in molecular mass. Furthermore, the αHL, OmpF, and OmpG protein nanopores cannot permit the passage of bulky biomolecules, such as folded proteins (17, 18) or even double-stranded DNA (dsDNA) (19).

To overcome these fundamental limitations, a larger monomeric β-barrel protein pore is required for single-molecule stochastic sensing of biomolecules, such as dsDNA, functional proteins, and their ensembles. We decided to explore the ferric hydroxamate uptake component A (FhuA), a monomeric β-barrel protein from the outer membrane of *Escherichia coli*. The high resolution x-ray crystal structure of FhuA is available, revealing a large membrane-spanning β-barrel domain, composed of 22 β strands (residues 161–714) (Fig. 1), which is filled by a globular N-terminal domain (residues 1–160) called the cork (20, 21). The barrel has an elliptically shaped cross-sectional area, and the sequential β strands run anti-parallel to one another, conferring an exceptional robustness (22–24). Adjacent β strands are connected by short turns on the periplasmic side and long loops on the extracellular side (Fig. 1). The x-ray

* This work was supported, in whole or in part, by National Institutes of Health Grant R01 GM088403 (to L. M.). This work was also supported by Grants DMR-0706517 and DMR-1006332 from the National Science Foundation (to L. M.).

[S] The on-line version of this article (available at http://www.jbc.org) contains supplemental Figs. S1–S8 and references.

[1] Both authors contributed equally to this work.

[2] To whom correspondence should be addressed: Dept. of Physics, Syracuse University, 201 Physics Bldg., Syracuse, NY 13244-1130. Tel.: 315-443-8078; Fax: 315-443-9103; E-mail: lmovilea@physics.syr.edu.

[3] The abbreviations used are: αHL, α-hemolysin; S, siemens; OG, *n*-octyl β-D-glucopyranoside; DDM, *n*-dodecyl β-D-maltoside; oPOE, octyl-polyoxoethylene.

TABLE 1
Comparison of structural features of various β-barrel membrane proteins

Protein	Protein Data Bank code	Lumen occlusions	No. of β strands	Diameter	Functional unit	Refs.
				nm		
αHL	7AHL	None	14	1.5	Heptameric	4
OprD	2ODJ	L3, L4, L7	18	0.5	Monomer	67
OpdK	2QTK	L3, L4, L7	18	0.8	Monomer	68
LamB	1MAL	Extracellular loops[a]	18	0.6	Trimer	69
OmpA	1BXW	None	8	1.0	Monomer	70
OmpF	2OMF	Extracellular loops[b,c]	16	1.2	Trimer	71
OmpG	2F1C	Gating loop[d]	14	2.0	Monomer	15
FecA	1KMO	Plug (87–223) 136	22	4.5 × 3.5[e]	Monomer	72
FepA	1FEB	N-terminal plug (1–153) 153	22	4.0 × 3.0[e]	Monomer	73
BtuB	1NQH	N-terminal plug (6–132) 127	22	4.2 × 3.7[e]	Monomer	74, 75
PapC	3FIP	Various structures[f,g,h]	24	4.6 × 2.8[e]	Dimer	76
FhuA	1BY5	N-terminal plug (1–160) 160	22	3.9 × 4.6[e]	Monomer	21

[a] Inwardly folded loops (L1, L3, and L6) contribute to the constriction of ~1/2 through the channel.
[b] Loops 1 and 4–8 partially close entrance to the lumen.
[c] Loop 3 folds inward and constricts the lumen.
[d] Loop 6 is involved in the gating activity of the pore thereby reducing access to the lumen.
[e] Elliptical cross-sectional sides were determined using C^{α} positions.
[f] Plug (259–335) 77 residues.
[g] β-Hairpin (447–465) 19 residues.
[h] α-Helix (230–240) 11 residues.

crystal structure of the FhuA protein indicates that, unlike porins, the extracellular loops do not fold back into the interior of the pore but rather project away from the membrane surface (20, 21). It has also revealed its monomeric character and elucidated the relatively clear architecture of the channel at the atomic level (Fig. 1) (20, 21). Therefore, this information paves the way for the use of this outer membrane protein in redesign studies and in the possible development of stochastic biosensing elements.

The FhuA protein exhibits a highly diverse functionality. Its primary role is to provide a binding site on the outer membrane surface for siderophores, such as ferrichrome (20, 21, 25). In addition, FhuA also serves as a transporter of the antibiotics albomycin and rifamycin (26, 27), as a receptor for the antimicrobial peptide microcin J25 (MccJ25) (28), a number of bacteriophages, including T1, T5, and φ80 (29–33), and the protein toxin colicin M (34). Furthermore, the dynamics of the wild-type FhuA (WT-FhuA) protein at an atomistic level has been revealed by molecular dynamics simulations (35). The FhuA channel exhibits a remarkable robustness, versatility, tractability, and thermal stability, as was well documented by prior spectroscopic and calorimetric studies (22–24).

In this study, we designed a series of single domain or multiple loop deletions to investigate which parts of the FhuA protein contribute to the occlusion of the lumen. First, we constructed a deletion mutant removing the cork domain, which encompassed the first 160 amino acids (FhuAΔ1–160) (Table 2). Second, we deleted 52% of strand β8 along with nine amino acids of loop L4 (FhuAΔ335–355). Third, we also deleted 52% of strand β8 along with most of loop L4 (FhuAΔ322–355), leaving the first seven amino acids. This construct will not have loop L4 deleted *per se*, but it might put a structural constraint on loop L4 to compensate for the loss of the majority of the β strand in the barrel (supplemental Fig. S2). Loop L4 is targeted for modifications, because it has been shown to reduce the extracellular entrance to the lumen of FhuA protein by ~50% (20), and perhaps it would prevent more modulation or even the release of the cork upon the application of a transmembrane potential.

Previously engineered FhuA proteins were stable and functional in reconstituted systems, as judged by their channel-forming ability in planar lipid membranes (36–39). In the past, these deletion mutants were studied by macroscopic electrical recordings, in which detailed, time-resolved single-channel information about each deletion mutant is lacking. For example, the channel sub-states can be difficult to decipher (36, 39). Thus, these macroscopic current studies hindered important conclusions about which parts of FhuA occlude the lumen. Therefore, we used single-channel electrical recordings to investigate single-deletion FhuA mutants along with the WT-FhuA protein to derive detailed information about their spontaneous, stochastic gating.

In addition to single-deletion FhuA mutants, we examined double and multiple deletion mutants to obtain a comprehensive picture of the cumulative effect of both the cork domain and several large extracellular loops on the biophysical features of the FhuA protein. Based upon examination of the crystal structure of the FhuA protein (20, 21), our major hypothesis was that L4 is not the only loop occluding the pore, but other extracellular loops may modulate the unitary conductance of the cork-free FhuA protein. We found that the removal of the cork domain and loop L4 produces an increase in the single-channel conductance up to ~3.0 nS over WT-FhuA. In accord with our expectations, the deletion of additional extracellular loops (L3, L4, L5, and L11) resulted in a substantially enhanced single-channel conductance of ~4.8 nS. To our knowledge, this is the highest single-channel conductance ever measured with an engineered FhuA protein (29, 36–39). The cork-free, multiple loop-deletion FhuA (FhuAΔC/Δ4L) proteins were either extracted from outer membranes or refolded from inclusion bodies (Fig. 1). Remarkably, high resolution single-channel electrical recordings accomplished with planar lipid bilayers showed that, although their unitary conductance is closely similar, membrane-extracted and refolded FhuAΔC/Δ4L proteins exhibit slightly different single-channel signatures. This finding pinpoints the power of single-channel electrical measurements in detecting subtle functional distinctions of membrane protein channels.

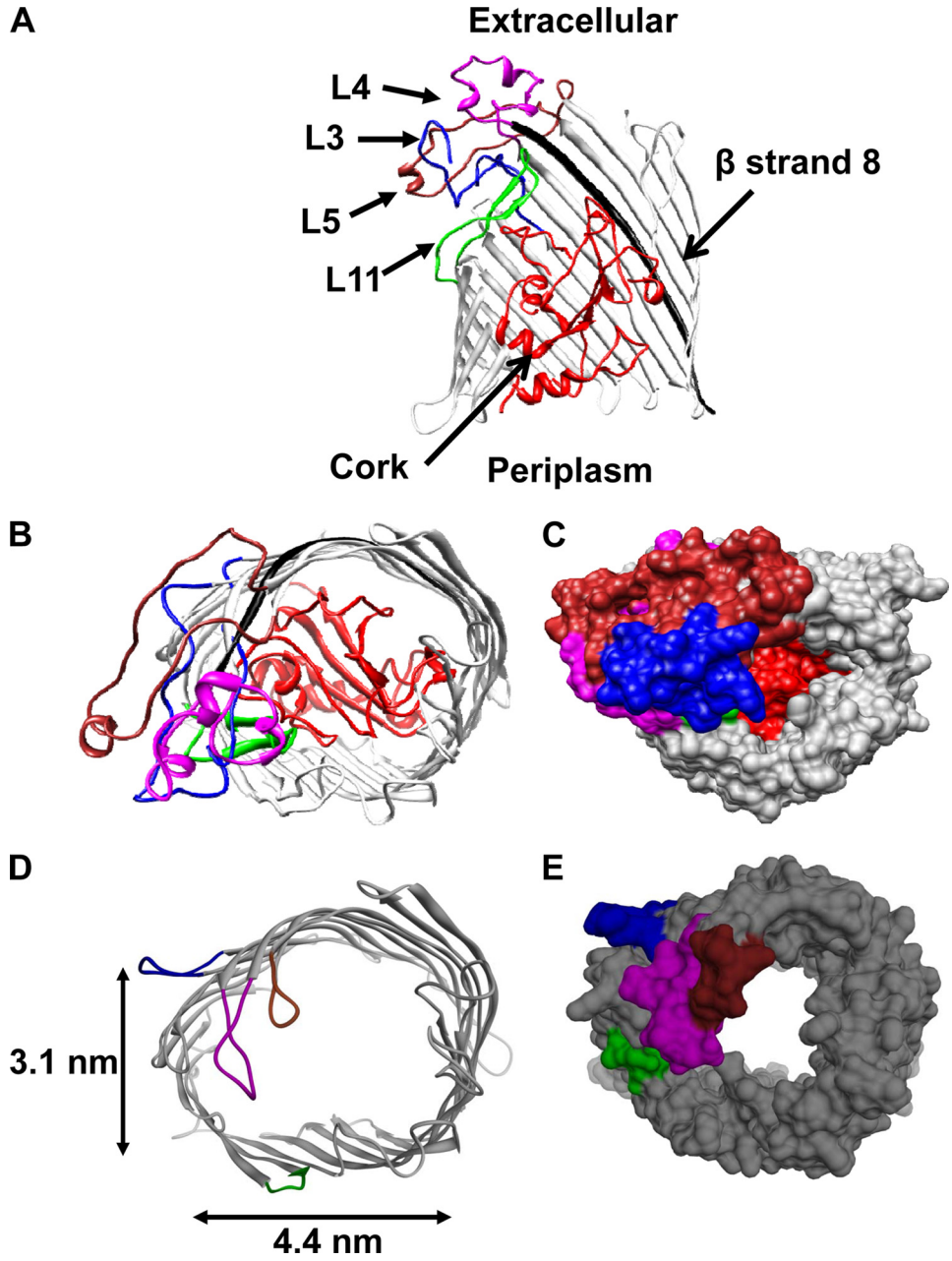

FIGURE 1. **Structure of the FhuA protein.** *A,* ribbon diagram of the WT-FhuA protein (*side view*). Domains that were targeted for modifications in this study are the following: loops L3 (*blue*), L4 (*magenta*), L5 (*brown*), L11 (*green*), the first 160 amino acids, the cork (*red*), and strand β8 in the barrel (*black*). *B,* extracellular view of the WT-FhuA protein. *C,* surface representation of the extracellular view of the WT-FhuA protein, showing that the cork domain completely fills the pore lumen. *D,* ribbon diagram of the engineered FhuAΔC/Δ4L protein viewed from the extracellular side. *E,* surface representation of the engineered FhuAΔC/Δ4L protein.

EXPERIMENTAL PROCEDURES

Plasmid Constructs—pPR-IAB1 plasmids that contained *wt fhua* and *fhuaΔ1–160*, with an internal 6×His$^+$ cloned into the coding region for the surfaced-exposed loop L5, were gifted by Professor Ulrich Schwaneberg (Jacobs University Bremen, Bremen, Germany). To construct *fhuaΔ322–355,* inverse PCR was performed on the *wt fhua*-containing plasmid with the following two phosphorylated primers: p-322, 5′-GTG ATC GAA GCT GTA GCC GAC-3′, and p-355, 5′-AAT GCT TAC AGC AAA CAG TGT-3′. The resulting PCR products were gel-purified using the MinElute® gel purification kit (Qiagen, Germantown, MD) and then self-ligated with T4 DNA ligase. To construct *fhuaΔ335–355*, the same strategy was applied except that p-322 was exchanged with p-335, 5′-GCG CAG GTT CTG ACG CAC AGT-3′. To construct *fhuaΔ1–160/Δ322–355* and *fhuaΔ1–160/Δ335–355*, we applied the above overall strategy except that we performed inverse PCR on the *fhuaΔ1–160*-containing plasmid. All constructs were verified by DNA sequencing. The *fhua* gene, which lacked the regions coding for the cork domain and loops 3–5 and 11, named *fhuaΔC/Δ4L*, was constructed by *de novo* synthesis (GENEART, Regensburg, Germany) in the pMK-RQ plasmid flanked by EcoRI and XhoI restriction sites. In this construct, the deleted loops were replaced with the polypeptide NSEG(S). A serine residue was

TABLE 2
The physical properties of the extracellular loops of the FhuA protein

Loop	Overall charge[a]	Charge ratio[b]	Residues	Loop length[c]	Comments[d]
				Å	
L1	−1	0/−1	Thr^{170}–Ser^{172}	7.0	Very short loop
L2	+1	+1/0	Ala^{203}–Ser^{208}	17.5	Short loop
L3	0	+4/−4	Tyr^{243}–Asn^{273}	105	Large flexible, random coil loop that folds back into the pore lumen
L4	+1	+3/−2	Cys^{318}–His^{339}	73.5	Large loop that contains three helices, and a β strand. The loop also contains a stabilizing disulfide bridge Cys^{318}–Cys^{329}. L4 along with part of the β strands block the access to the pore lumen
L5	−4	+3/−7	Asp^{394}–Asn^{419}	87.5	Large loop that contains a β strand, which partially occludes the pore lumen
L6	+1	+1/0	Arg^{463}–Gly^{466}	10.5	Very short loop
L7	0	+1/−1	Pro^{502}–Pro^{515}	45.5	Flexible loop that does not appear to enter or block the pore lumen
L8	−2	0/−2	Asp^{552}–Phe^{559}	24.5	Short loop
L9	+1	+2/−1	Asp^{598}–Lys^{611}	45.5	Medium sized flexible loop. The movement of L9 does appear to be restricted due to its positioning between two uneven β strands
L10	0	+1/−1	Gly^{640}–Ser^{654}	49.0	Medium sized flexible loop that has potential to block the pore lumen
L11	−2	+1/−3	Asn^{682}–Arg^{704}	77.0	Large loop that contains an anti-parallel β sheet, which protrudes into the pore lumen

[a] The total charge of the loop was calculated at pH 7.4.
[b] The total number of positive charges of the loop *versus* its negative charges and was calculated at pH 7.4.
[c] The length of the loop under the stretched out conformation was based upon the total number of residues.
[d] Comments concern the cork-free FhuA protein.

added, if it did not exist in the original loop (40). The pMK-RQ plasmid was digested with EcoRI and XhoI enzymes, and the released *fhuaΔC/Δ4L* gene was gel-purified, as mentioned above, and cloned into the pPR-IBA1 expression plasmid. This latter plasmid was also digested with EcoRI and XhoI enzymes. A C-terminal 6×His^+ tag, which was preceded by a thrombin protease cleavage site, was added to *fhuaΔC/Δ4L* by inverse PCR utilizing the following two primers: 5′-ACT ACC GCG TGG CAG CAG AAA ACG **AAA GGT TGC GGT GGC AAC**-3′ and 5-CAT CAT CAC CAT CAC CAC TAA AGC GCT GGG AGC CCC CCC AGT-3′. The thrombin cleavage site and 6×His^+ tag coding sequences are boldface and underlined, respectively. The final plasmid was checked by DNA sequencing.

Protein Expression—pPR-IBA1 containing the *fhua* gene and its derived constructs were transformed into *E. coli* BL21 (DE3) omp9 (F^- $hsdS_B$ (r_B^- m_B^-) *gal ompT dcm* (DE3) Δ*lamB ompF*::Tn5 Δ*ompA* Δ*ompC ompN*::Ω (kindly provided by Dr. Helge Weingart, Jacobs University Bremen). The transformed cells were then grown in 2× TY media at 37 °C, until an A_{600} ~0.7–0.8. Protein expression was induced with isopropyl β-D-1-thiogalactopyranoside, at a final concentration of 1 mM, and allowed to continue until the cell growth plateaued, as measured by A_{600} ~1.4.

Purification of the Wild-type FhuA Protein—The wild-type FhuA (WT-FhuA) protein was purified as described previously (41) with the following modifications. The outer membranes were pre-extracted in 20 mM Tris, 1 mM EDTA, 0.1% octylpolyoxoethylene (oPOE), pH 8.0. The membrane-extracted proteins were obtained by incubating the outer membranes for 1 h at 37 °C, while shaking at 200 rpm, in 20 mM Tris, 1 mM EDTA, 3% oPOE, pH 8.0. The insoluble materials were sedimented by centrifugation at 50,000 × *g* for 45 min at 4 °C; the supernatant, enriched in extracted outer membrane proteins, was used for subsequent purification steps.

Prior to starting purification, the detergent concentration of the solubilized WT-FhuA was reduced from 3 to 1% to lessen the effects of detergent screening during chromatographic separation. Lower concentrations of oPOE were also tested; however, the concentrations were determined to be below the critical micelle concentration and thus did not allow for complete solubilization of the WT-FhuA protein. Following the decrease of the detergent concentration, the samples were loaded onto an UNO-Q strong anion exchange column (Bio-Rad) equilibrated with 25 mM Tris, 20 mM EDTA, 1% oPOE, pH 7.8, and eluted with 250–300 mM NaCl. The FhuA-containing fractions were then pooled and concentrated (Amicon 30K MWCO). In preparation for metal affinity chromatography, the buffer was exchanged, using a Bio-Select 250–5 SEC column (Bio-Rad), to 300 mM KCl, 50 mM KH_2PO_4, 5 mM imidazole, 1% oPOE, pH 8.0. FhuA-containing fractions were pooled and loaded onto an immobilized metal affinity column (Bio-Rad), equilibrated with 300 mM KCl, 50 mM KH_2PO_4, 5 mM imidazole, 1% oPOE, pH 8.0. The column was washed with 10 mM imidazole, and the bound proteins were eluted with 250 mM imidazole, analyzed by SDS-PAGE, and used for single-channel electrical recordings (supplemental Fig. S3).

Purification of the Single- and Double-Deletion FhuA Proteins—Briefly, cells expressing FhuA proteins Δ322–355 and Δ335–355 were resuspended in PBS (0.9% NaCl, 1 mM potassium phosphate, pH 7.3). FhuA proteins Δ1–160, Δ1–160/Δ322–355, and Δ1–160/Δ335–355 were resuspended in 20 mM NaH_2PO_4, pH 7.4. The cells were disrupted using either a Sonic Dismembrator model 500 (ThermoFisher, Waltham, MA) or a microfluidizer (Microfluidics, Newton, MA), after which the lysates were centrifuged at 8,500 × *g* for 20 min at 4 °C. The supernatant was then centrifuged at 180,000 × *g* for 1 h at 4 °C. The pelleted total membranes were then resuspended in Triton/urea buffer (50 mM Tris-HCl, 6 M urea, 2% Triton X-100, pH 8.0) or 20 mM NaH_2PO_4, 2% *n*-laurylsarcosine, pH 7.4, to solubilize the inner cell membranes. This was followed by rolling incubation at room temperature for 2 h and then centrifugation at 180,000 × *g* for 1 h at 4 °C. The outer membrane pellet was then resuspended in *n*-octyl β-D-glucopyranoside (OG)/EDTA buffer (50 mM Tris-HCl, 1 mM EDTA, 33 mM OG, pH 8.0) or 20 mM NaH_2PO_4, 33 mM OG, pH 7.4, and rotated overnight. The suspension was then centrifuged at 180,000 × *g* for 1 h at 4 °C. The solubilized FhuA proteins Δ322–355, Δ335–355, Δ1–160/Δ322–355, and Δ1–160/Δ335–355 were then purified by ion exchange chromatography as in WT-FhuA

except with OG-containing buffers, followed by size exclusion chromatography (supplemental Fig. S3). We performed immobilized metal affinity column purification with the above proteins but did not get the proteins bound to the column, presumably due to the 6×His^+ tag not being accessible.

For FhuAΔ1–160, the protein was purified utilizing the 6×His^+ tag (42). The FhuAΔ1–160-containing supernatant was loaded onto a Ni^{2+}-nitrilotriacetic acid column (Qiagen), equilibrated in NPI-10 (300 mM NaCl, 50 mM NaH_2PO_4, 33 mM OG, 10 mM imidazole, pH 8.0). After washing the column with 6 column volumes with NPI-10 buffer, followed by a 6-column volumes wash with NPI-20 (300 mM NaCl, 50 mM NaH_2PO_4, 33 mM OG, 20 mM imidazole, pH 8.0), the FhuA proteins were eluted in NPI-150 (50 mM NaH_2PO_4, 300 mM NaCl, 33 mM OG, 150 mM imidazole, pH 8.0). Purity of the FhuAΔ1–160 protein was assessed by SDS-PAGE (supplemental Fig. S3).

Purification of the FhuAΔC/Δ4L Protein—The harvested cells were resuspended in 50 ml of resuspension buffer (100 mM NaCl, 50 mM Tris-Cl, 10 mM $MgCl_2$, pH 8.0, supplemented by 10 μg/ml DNase I and EDTA free-Complete protease inhibitors) (Roche Applied Science). The resuspended cells were lysed using a microfluidizer (Microfluidics). The homogenate was centrifuged for 20 min (2,000 × *g*, 4 °C). The supernatant was then centrifuged for 1 h (180,000 × *g*, 4 °C) to pellet the total membranes. The resulting pellet was then resuspended in resuspension buffer and centrifuged again for 1 h (180,000 × *g*, 4 °C). The washed membrane-containing pellet was then suspended in *n*-laurylsarcosine-containing buffer (100 mM NaCl, 50 mM Tris-Cl, 2% *n*-laurylsarcosine (w/v), pH 8.0) and rotated overnight at 4 °C to selectively solubilize the inner membranes. The suspension was then ultracentrifuged for 1 h (180,000 × *g*, 4 °C). The outer membrane containing pellet was resuspended in deionized double-distilled H_2O and ultracentrifuged for 1 h (180,000 × *g*, 4 °C). This step was repeated twice to ensure the elimination of residual detergent from the outer membrane-containing pellets. The washed pellets were then resuspended in outer membrane solubilization buffer (1% OG or 0.5% *n*-dodecyl β-D-maltoside (DDM), 100 mM NaCl, 50 mM Tris-Cl, 10 mM DTT, 0.1 mg/ml lysozyme, pH 8.0). The suspension was first rotated for 1 h at room temperature, followed by overnight rotation at 4 °C, and then ultracentrifuged for 1 h (at 180,000 × *g*, 4 °C) to separate the insoluble debris from solubilized outer membrane protein (FhuAΔC/Δ4L). The OG- or DDM-solubilized FhuAΔC/Δ4L was checked by SDS-PAGE and then stored at −80 °C.

23 ml of solubilized FhuAΔC/Δ4L was incubated with 2 ml of Ni^{2+}-nitrilotriacetic acid resin (equilibrated in 500 mM NaCl, 20 mM Tris-HCl, 1% OG or 0.5% DDM, pH 8.0) for 12 h at 4 °C while rotating. The resin was then collected in a 30-ml column and washed with 5 column bed volumes of 500 mM NaCl, 20 mM Tris-HCl, 1% OG or 0.5% DDM, pH 8.0, followed by 5 column bed volumes of 500 mM NaCl, 20 mM Tris-HCl, 10 mM imidazole, 1% OG or 0.5% DMM, pH 8.0, and finally eluted in 5 bed volumes of 500 mM NaCl, 20 mM Tris-HCl, 250 mM imidazole, 1% OG or 0.5% DDM, pH 8.0. The FhuAΔC/Δ4L-enriched fractions were pooled and ultraconcentrated by 30K M_r cutoff ultraconcentrators (Sartorius Stedim Biotech, Goettingen, Germany) and checked by SDS-PAGE (supplemental Fig. S3).

Refolding of the FhuAΔC/Δ4L Protein from Inclusion Bodies—The harvested cells were then suspended in 50 ml of resuspension. The cells were then lysed using a microfluidizer (Microfluidics). The homogenate was then centrifuged for 10 min at 2,000 × *g*, 4 °C, to remove unbroken cells. The supernatant was then centrifuged at 30,000 × *g* to pellet the inclusion bodies. The resulting pellet (inclusion bodies) was then resuspended in washing buffer (PBS, 1% Triton X-100, 1 mM EDTA, pH 7.4). The resuspended inclusion bodies were then centrifuged at 30,000 × *g* for 30 min at 4 °C. The washing step was repeated twice, and the resulting inclusion bodies were used for the subsequent refolding protocol.

The inclusion bodies were resuspended in denaturing buffer (100 mM NaCl, 50 mM Tris-HCl, 8 M urea, pH 9.0) to a concentration of 15 mg/ml. Urea-assisted denaturation and solubilization was allowed to continue by rotating overnight at the ambient temperature. This was followed by clarification by centrifugation (30,000 × *g* for 30 min at 4 °C). The clarified supernatant was loaded onto a Bio-Scale Mini Profinity™ immobilized metal affinity column cartridge (Bio-Rad) equilibrated in denaturing buffer. After washing the column five times, the concentration of denaturing buffer was linearly decreased, although the concentration of refolding buffer (50 mM Tris-HCl, 3 mM DTT, 1 mM EDTA, 79 mM urea, 1.23% (w/v) DDM, pH 8.0) was linearly increased, followed by an incubation period of 24 h. The detergent concentration was then decreased with washing buffer (50 mM Tris-HCl, 1 mM EDTA, 0.25% (w/v) DDM, pH 8.0). Proteins were eluted with elution buffer (250 mM imidazole, 50 mM Tris-HCl, 1 mM EDTA, 1 M NaCl, 0.25% (w/v) DDM, pH 8.0).

The eluted fractions were then checked by SDS-PAGE and stained with Invision His tag stain (Invitrogen), followed by colloidal blue staining using GelCode blue stain reagent (ThermoFisher). The FhuAΔC/Δ4L-containing fractions were then pooled and concentrated, and the NaCl concentration was decreased using centrifugal filtration. The concentrated proteins were then loaded onto a Mono Q column (Bio-Rad) equilibrated with washing buffer (50 mM Tris-HCl, 1 mM EDTA, 0.25% (w/v) DDM, pH 8.0). A linear gradient of elution buffer (1 M NaCl, 50 mM Tris-HCl, 0.25% (w/v) DDM, pH 8.0) was applied, and the unfolded FhuAΔC/Δ4L protein eluted first at ~75 mS/cm, although the folded FhuAΔC/Δ4L protein eluted as a second peak at ~350 mS/cm (43).

Electrical Recordings on Planar Lipid Bilayers—Electrical recordings were carried out utilizing planar bilayer lipid membranes (44–46). The *cis* and *trans* chambers (1.5 ml each) of the apparatus were separated by a 25-μm-thick Teflon septum (Goodfellow Corp., Malvern, PA). An aperture in the septum, ~80–120 μm in diameter, was pretreated with hexadecane (Sigma) dissolved in highly purified pentane (Fisher HPLC grade, Fair Lawn, NJ) at a concentration of 10% (v/v). A 1,2-diphytanoyl-*sn*-glycerophosphatidylcholine (Avanti Polar Lipids, Alabaster, AL) bilayer was formed across the aperture. The WT-FhuA and FhuA mutants were introduced by adding purified proteins to a final protein amount of 100–180 ng. Single-channel currents were recorded using an Axopatch 200B patch clamp amplifier (Axon Instruments, Foster City, CA) connected to Ag/AgCl electrodes through agarose bridges. The *cis*

TABLE 3

Comparison of the conductance between the WT-FhuA protein and its deletion mutants

The unitary conductance was obtained from single channel electrical recordings in 1 M KCl, 10 mM phosphate, pH 7.4. The applied transmembrane potential was +40 mV.

Protein	Conductance
	nS
WT-FhuA	0.3 ± 0.2 (n = 4)
FhuA Δ1–160	2.5 ± 0.6 (n = 4)
FhuA Δ335–355	3.1 ± 0.2 (n = 3)
FhuA Δ1–160/Δ335–355	3.0 ± 0.5 (n = 3)[a]
FhuA Δ1–160/Δ322–355	3.0 ± 1.5 (n = 4)[b]
mFhuA ΔC/Δ4L	4.8 ± 1.3 (n = 58)
rFhuA ΔC/Δ4L	4.9 ± 0.7 (n = 25)

[a] The conductance measurements were derived from the peak that corresponds to the most probable conductance in all-points current amplitude histogram (Fig. 3*A*, *right panel*).

[b] The conductance measurements were derived using the S_3 sub-state in the all-points current amplitude histogram (Fig. 3*B*, *right panel*).

chamber was grounded so that a positive current (upward deflection) represents a positive charge moving from the *trans* to *cis* side. A Dell Optiplex Pentium PC (Dell Computers, Austin, TX) was equipped with a DigiData 1322A A/D converter (Axon) for data acquisition. The signal was low-pass filtered with an 8-pole Bessel filter (model 900; Frequency Devices, Ottawa, IL) at a frequency of 10 kHz and sampled at 100 kHz, unless otherwise stated. For data acquisition and analysis, we used the pClamp10.1 software package (Axon).

RESULTS

Single-channel Electrical Signatures of the FhuA Protein and Its Single-Deletion Mutants—When the WT-FhuA protein was reconstituted into a planar lipid bilayer, we observed a single-channel conductance of 0.3 ± 0.2 nS (n = 4 distinct single-channel experiments) at an applied membrane potential of +40 mV in 1 M KCl, 10 mM potassium phosphate, pH 7.4 (Table 3). Fig. 2*A*, *left panel*, shows a representative single-channel electrical trace recorded with the WT-FhuA protein. Fig. 2*A*, *right panel*, presents an all-points current amplitude histogram of the single-channel electrical trace illustrated in the *left panel*. This all-points current amplitude histogram identifies a current amplitude peak located at ~12.5 pA.

To redesign an open FhuA protein pore, the cork domain was removed (Fig. 1*A*). The expectation was that the removal of the cork domain should lead to a protein with a hollow lumen, forming a high conductance channel. Surprisingly, the single-channel current fluctuated between low conductance (0.2 ± 0.1 nS, n = 4) and high conductance (2.5 ± 0.6 nS, n = 4) current sub-states, S_1 and S_2, respectively (Fig. 2*B* and Table 3). Throughout this work, the assignment of different conductance sub-states relied on all-points current amplitude Gaussian histogram peaks (*e.g.* Fig. 2*B*, *right panel*). These two current sub-states are not generated from multiple channels but rather from one protein. If the trace observed with the FhuAΔ1–160 protein channel is produced by two different single-channel conductance proteins, then we should have been able to see more independent small and large conductance openings of this mutant. This is not the case. We observed that S_2 occurred frequently after S_1. We rarely noticed S_1 or S_2 independently (0 to ~25 to 0 pA or 0 to ~100 to 0 pA, respectively). Taken together, it is likely that S_1 and S_2 are different open current sub-states of the same FhuAΔ1–160 protein pore. For example, the 5th last opening (Fig. 2*B*, *expanded trace*) is featured by a current amplitude that is the sum of the small and large opening. However, in this event, the current increases to the maximum value without having a discrete step at S_2. First, if this event was characteristic of the opening of two channels, it should show a discrete opening to the S_2 sub-state, followed by another low amplitude current step. This is not the case. Other closely similar events, but of greater current amplitude than the sum of the small and large opening, were noticed (supplemental Fig. S4).

Killman *et al.* (38), using macroscopic current measurements, showed that FhuAΔ335–355 exhibits an open pore. Therefore, this deletion mutant was examined using time-resolved single-channel electrical recordings. Specifically, we wished to know whether the alteration of loop L4 impacts the gating fluctuations of the WT-FhuA protein (Fig. 1). Single-channel electrical recordings with the FhuAΔ335–355 protein agreed with the prior exploration of this mutant (38). Fig. 2*C* shows a representative single-channel electrical trace obtained with FhuAΔ335–355. This electrical trace reveals an open sub-state S_2, with a single-channel conductance of 3.1 ± 0.2 nS (n = 3), accompanied by frequent short lived gating events reaching a current sub-state S_1, with a single-channel conductance 1.9 ± 0.2 nS (n = 3). To obtain a better understanding of the current fluctuations produced by loop L4, we also examined the deletion mutant FhuAΔ322–355. This mutant produces a channel with multiple open states within a very broad range of the single-channel conductance (supplemental Fig. S5). The observed maximum single-channel conductance was ~3.5 nS, indicating that further shortening of loop L4 results in a more fluctuating structure of the FhuA protein.

Single-channel Electrical Signatures of the Double-Deletion FhuA Mutants—Our analysis of the FhuAΔ1–160 protein indicated that the removal of the cork domain does not result in an open pore with a single unitary conductance. Furthermore, it is possible that loop L4 occludes the lumen (38). Therefore, we were interested in investigating the removal of both the cork domain (residues 1–160) and part of loop L4 (residues 335–355). When FhuAΔ1–160/Δ335–355 was explored by electrical recordings, an open channel was observed with an average single-channel conductance of 3.0 ± 0.5 nS (n = 3) (Fig. 3*A* and Table 3), which is in accord with previous studies of this protein (39). In contrast to other FhuA derivatives examined in this work, the current noise is exceptionally high, whereas the current showed a "wavy" behavior (Fig. 3*A*). Fig. 3*A* shows a longer time scale of the trace to reveal the specific signature of this double-deletion FhuA mutant. We were not able to assign individual conductance sub-states to FhuAΔ1–160/Δ335–355. The all-points histogram was only used to extract the most probable current sub-state of this FhuA derivative. Similar to FhuAΔ1–160/Δ335–355, FhuAΔ1–160/Δ322–355 produces a channel with a single-channel conductance of 3.0 ± 1.5 nS (n = 4) (Fig. 3*B* and Table 3). The fundamental difference between FhuAΔ1–160/Δ335–355 and FhuAΔ1–160/Δ322–355 is the appearance of three discrete current sub-states of the latter protein channel (Fig. 3*B*), which undergoes transient closures with the following two dwell times: τ_1 = 0.6 ± 0.1 ms

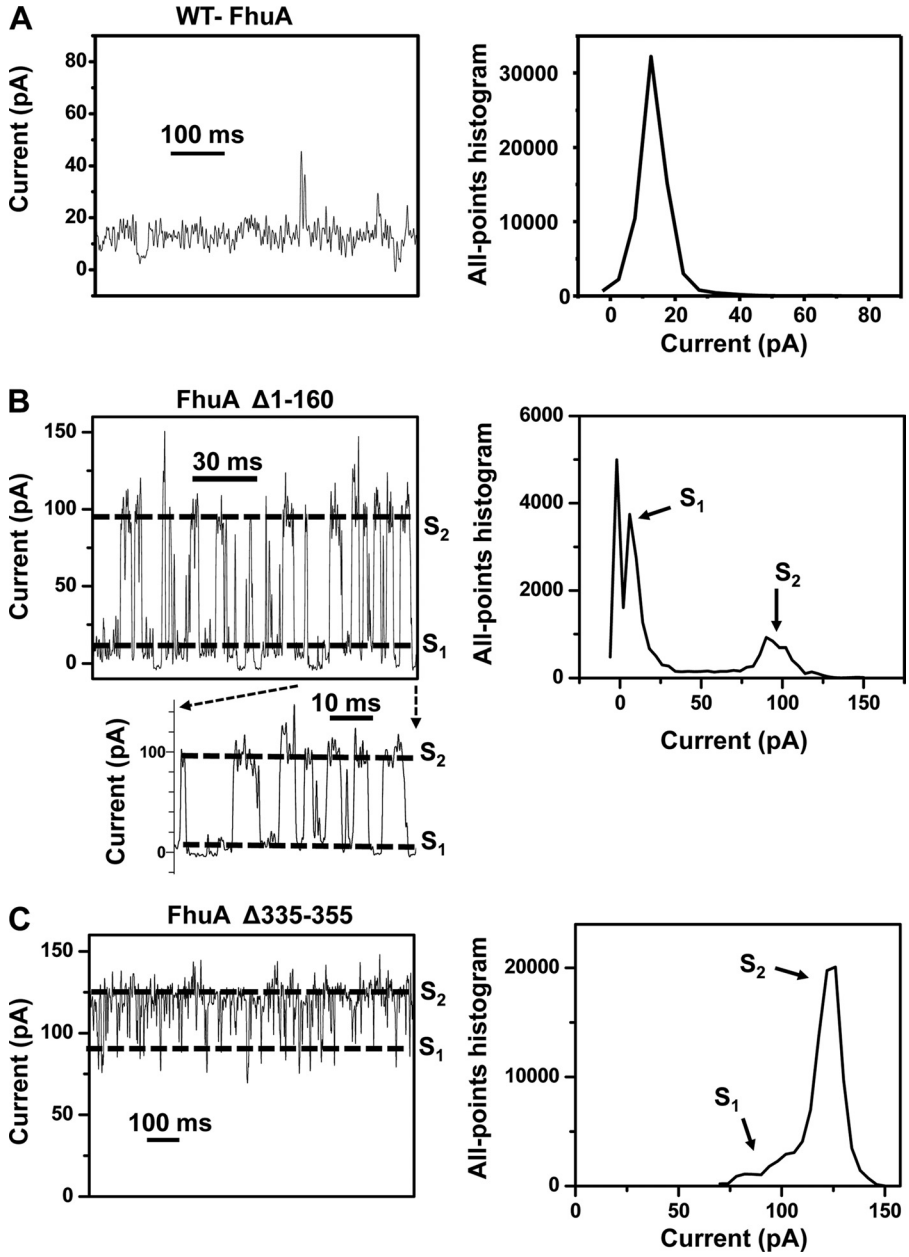

FIGURE 2. **Representative single-channel electrical recordings with the wild-type (WT-FhuA) and single-deletion mutants of FhuA protein.** *A*, WT-FhuA; *B*, FhuAΔ1–160; *C*, FhuAΔ335–355. The *dashed lines* indicate the current levels for the open (S_2) and gated (S_1) sub-states in *B* and *C*. *Right panels* show all-point current amplitude Gaussian histograms with the most probable sub-states of the channels. The *expanded trace* illustrates the last 60 ms of the trace from *B* at a greater time resolution. The *dashed lines* were assigned based upon the peaks from the all-points current amplitude Gaussian histograms from the *right panels* of *B* and *C*. The buffer solution was 1 M KCl, 10 mM potassium phosphate, pH 7.4. The transmembrane potential was +40 mV. Single-channel electrical traces were filtered at 1 kHz.

($P_1 = 0.37 \pm 0.01$) and $\tau_2 = 3.0 \pm 0.1$ ms ($P_2 = 0.63 \pm 0.01$) ($n = 4$) and with the overall event frequency of $201 \pm 93\ s^{-1}$. Throughout this work, the fits were based upon log likelihood ratio tests (47, 48), with a given confidence level of 0.95.

Single-channel Electrical Signatures of the Membrane-extracted, Multiple Deletion Mutant FhuAΔC/Δ4L—Inspection of the crystal structure of FhuA (20, 21) indicated that three additional loops can be folded back into the interior of the pore. We identified loops L3, L5, and L11 for further modification (Fig. 1*A*). These loops were chosen based on their length and spatial orientation in the FhuA crystal structure (Fig. 1*A* and Table 2). Furthermore, our protein structure prediction for double-deletion mutants has shown that these loops significantly obstruct the entrance to the pore lumen (supplemental Fig. S6, *A* and *B*). To prevent these loops from folding back into the pore lumen, we decided to redesign the FhuA protein with the following deletions: L3 (residues Tyr^{243}–Asn^{273}), L5 (residues Asp^{394}–Asn^{419}), L11 (residues Asn^{682}–Arg^{704}) along with L4 (residues Cys^{318}–His^{339}), and the cork domain (residues Met^{1}–Pro^{160}), leaving β-strand 8 unmodified. All loops were replaced with short turns, encompassing the sequence NSEGS (see under "Experimental Procedures") (40). The resulting engineered protein, called mFhuAΔC/Δ4L, was extracted from the outer membranes of *E. coli*. The average cross-sectional

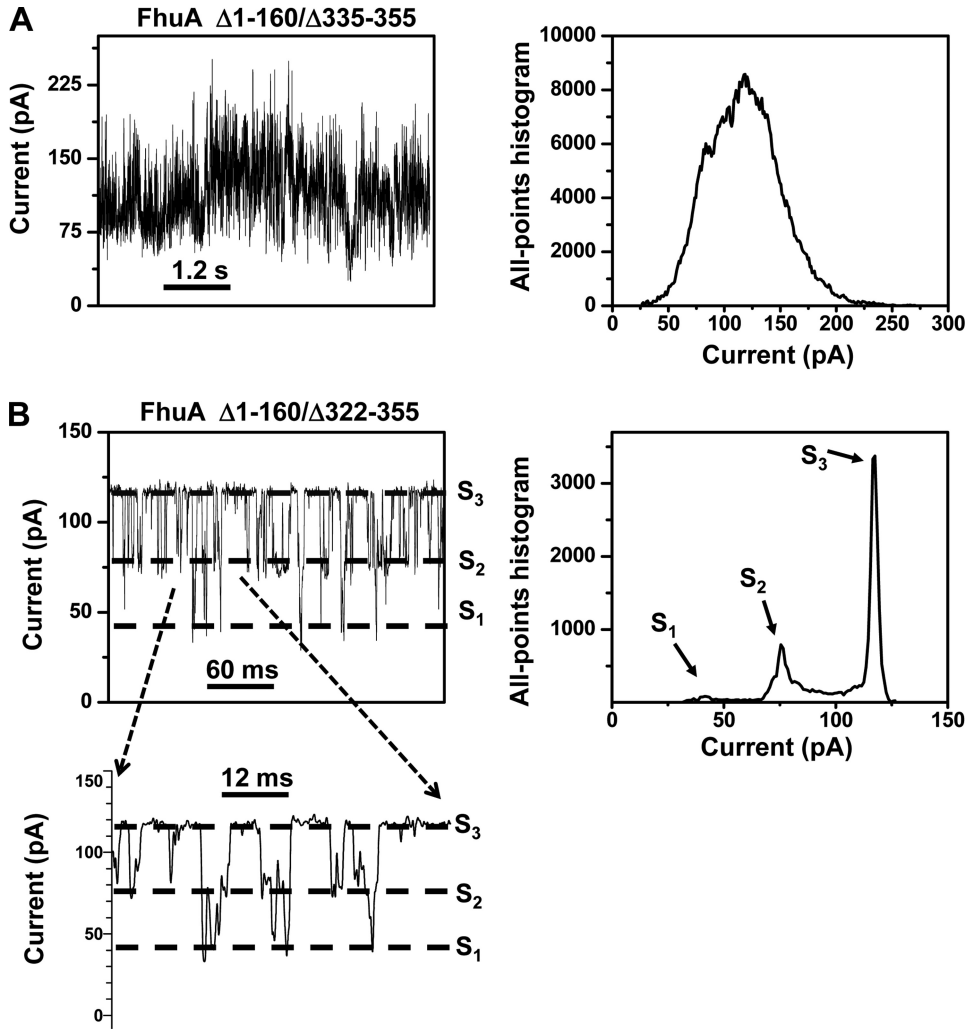

FIGURE 3. **Typical single-channel recordings for FhuAΔ1–160/Δ335–355 (*A*) and FhuAΔ1–160/Δ322–355 (*B*).** The *dashed lines* indicate the current levels for the three observed current states S_1, S_2, and S_3 in *B*. *Right panels*, all-point amplitude Gaussian histograms showing the most probable conductance states of the channels. The expanded trace in *B* shows a 60-ms trace at a greater time resolution. The *dashed lines*, which indicate different sub-states of the channel, were assigned based upon the peaks from the all-points current amplitude Gaussian histogram in the *right panel* of *B*. The buffer solution was 1 M KCl, 10 mM potassium phosphate, pH 7.4. The transmembrane potential was +40 mV. Single-channel electrical traces were filtered at 1 kHz.

surface and internal molecular volume of mFhuAΔC/Δ4L are 8.64×10^3 Å^2 and 38.1×10^3 Å^3, respectively, as calculated by using the CASTp software (49). These estimates were made with the assumption that the remaining FhuA structure is unmodified by these major cork and loop deletions.

The remaining unmodified loops L1, L2, L6, L7, L8, L9, and L10 featured 3, 6, 4, 14, 8, 14, and 16 amino acids in length (Table 2), respectively. L1, L2 and L6 are very short, and unlikely do fold into the pore lumen (supplemental Fig. S2, *left panel*). Lys^{508} in L7 is involved in a network of ion-pair interactions with Asp^{552} and Glu^{554} in L8 (supplemental Fig. S2, *right panel*). Recently, we have shown that these kinds of electrostatic interactions can stabilize the loops in a β-barrel protein pore (50). Therefore, we anticipated that these ion-pair interactions would prevent L7 and L8 from folding back into the pore lumen. L9 is stretched out between two highly asymmetric β strands, making a rigid structure and perhaps preventing L9 from folding back into the pore lumen (supplemental Fig. S2). Furthermore, L9 and L10 were not altered in the protein prediction studies (supplemental Fig. S6, *A* and *B*).

The mFhuAΔC/Δ4L protein exhibited pore forming activity as evidenced by a discrete stepwise increase of current of ~200 pA at a transmembrane potential of +40 mV (Fig. 4*A*). On some occasions (less than ~5%), we observed a pre-insertion activity of the mFhuAΔC/Δ4L protein pore (supplemental Fig. S7). Single-channels of the mFhuAΔC/Δ4L protein pore showed irresolvable and infrequent downward current spikes with the amplitude of 15–70% of the unitary current (Fig. 4*B* and *expanded trace*). We noticed that the mFhuAΔC/Δ4L protein pore is characterized by a single-channel conductance of 4.8 ± 1.3 nS ($n = 58$) at the transmembrane potential of +40 mV (Fig. 4*C* and Table 3). An alternative way to determine the single-channel conductance of the mFhuAΔC/Δ4L protein pore is to use the current *versus* voltage (I/V) curve (Fig. 4*D*). In this case, the slope of the I/V curve is exactly the single-channel conductance. We found that the single-channel conductance of mFhuAΔC/Δ4L pore is 5.7 nS in 1 M KCl, 10 mM potassium phosphate, pH 7.4, which falls within the standard error from the measurement using an applied transmembrane potential of +40 mV (Table 3). Furthermore, 67% of the channel conduc-

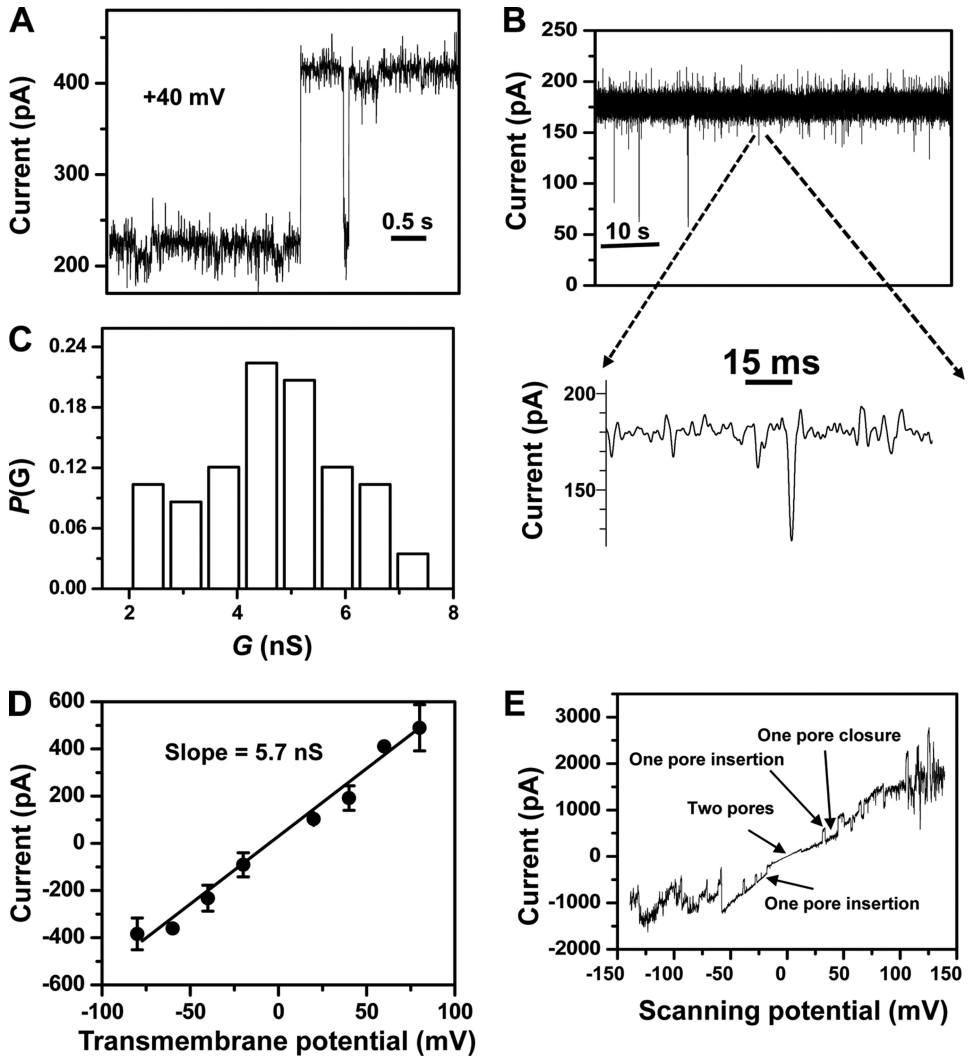

FIGURE 4. **Single-channel electrical recordings of the membrane-extracted FhuAΔC/Δ4L protein (mFhuAΔC/Δ4L).** *A,* step increase of the electrical current showing a single-channel insertion of the mFhuAΔC/Δ4L into the lipid bilayer. Protein was added to the *cis* side. The transmembrane potential was +40 mV. *B,* single-channel electrical trace of mFhuAΔC/Δ4L at an applied transmembrane potential of +40 mV. The *expanded trace* illustrates the signature of the channel at a greater time resolution. *C, histogram* of the probability (*P*(*G*)) of the occurrence of a given single-channel conductance of mFhuAΔC/Δ4L. *D,* current-voltage (I/V) relationship of a single mFhuAΔC/Δ4L protein pore. The standard *error bars* are determined from at least three separate single-channel experiments. *E,* voltage ramp acquired with two mFhuAΔC/Δ4L protein pores. Other pores either inserted or closed during the measurement at a greater transmembrane potential. The slope of the voltage ramp was 1.4 mV s^{-1}. Single-channel electrical recordings were performed in 1 M KCl, 10 mM phosphate buffer, pH 7.4. The single-channel electrical trace was low pass Bessel-filtered at 2 and 1 kHz in *B* and *E*, respectively.

tance values fall within the standard error of the average single-channel conductance (Fig. 4*C*). In Fig. 4*E*, we show the voltage-ramp recording, which is obtained with two mFhuAΔC/Δ4L protein pores inserted into the membrane. Insertions and closures of the mFhuAΔC/Δ4L protein pores are observed during the voltage-ramp recording. Generally, the channel was not stable at an applied transmembrane potential greater than 50 mV (Fig. 4*E*).

Refolded FhuAΔC/Δ4L Protein Forms a Channel That Is Closely Similar to the Channel Formed by the Membrane-extracted FhuAΔC/Δ4L Protein—The fundamental limitation of obtaining FhuAΔC/Δ4L from the outer membrane by using detergent extraction protocol is that a significant amount of expressed protein ends up in inclusion bodies (supplemental Fig. S8). Therefore, we pursued obtaining the refolded FhuAΔC/Δ4L (rFhuAΔC/Δ4L) protein pore from inclusion bodies using an improved and extensive on-column refolding protocol, which was followed by ion-exchange chromatography to separate folded from unfolded proteins ("Experimental Procedures").

We used two assays to monitor the refolding of the FhuAΔC/Δ4L protein, circular dichroism (CD) spectroscopy and single-channel electrical recordings. The CD spectrum of the rFhuAΔC/Δ4L protein showed a signature of high β-sheet-containing proteins with a large positive peak located at 196 nm and a well defined minimum located at 217 nm (Fig. 5*A*). This spectrum is similar to that of membrane-extracted WT-FhuA (51). To interpret the secondary structures present in the rFhuAΔC/Δ4L protein, web-assisted deconvolution of the CD spectrum (52, 53) was conducted using the CONTIN algorithm (54). The CD data analysis indicated the following protein structural content in rFhuAΔC/Δ4L: 40.8% β sheet, 3.7% α helix, 19.5% turns, and 37.2% disordered. Although the deconvolution of the CD spectrum of rFhuAΔC/Δ4L indicates that

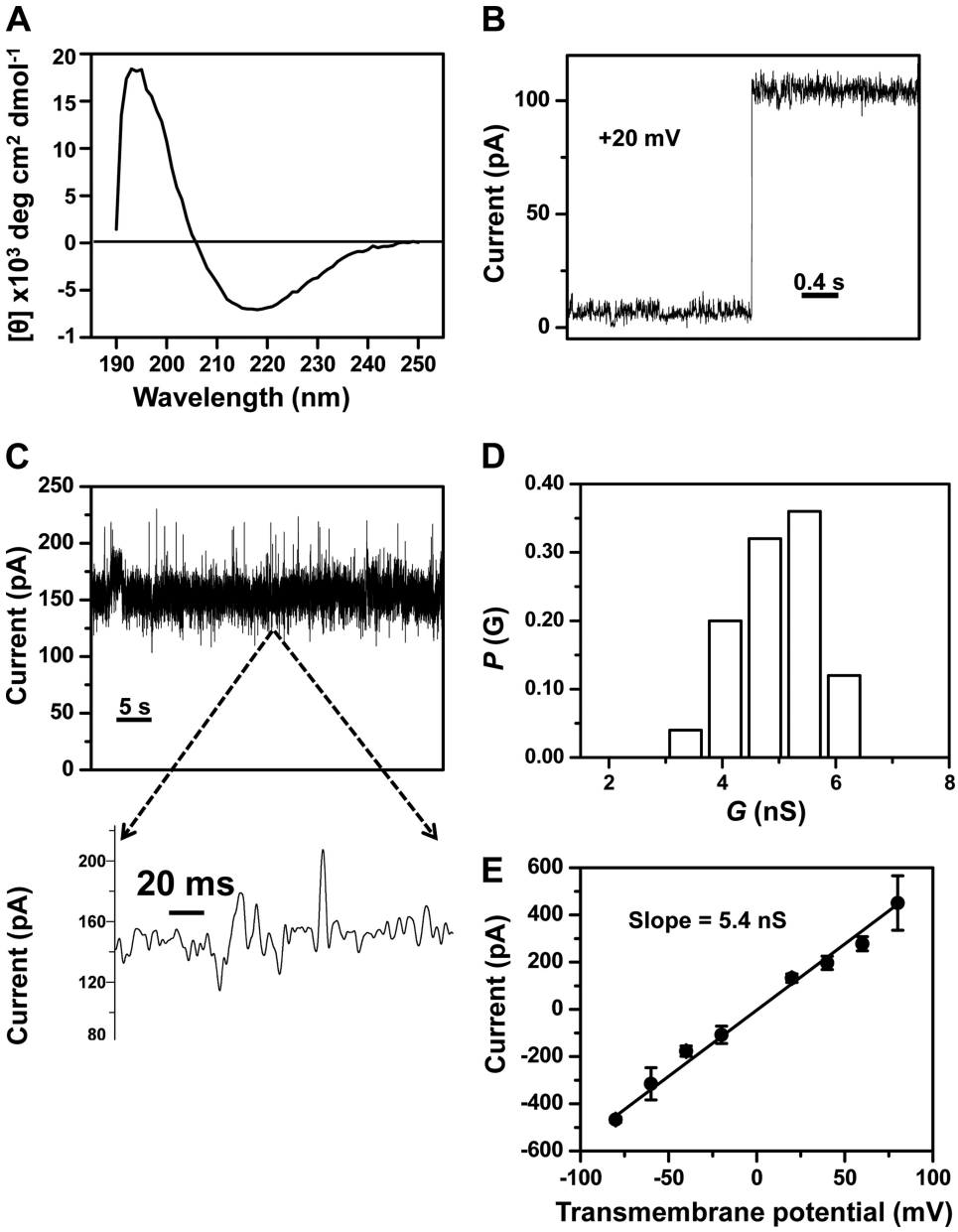

FIGURE 5. **Single-channel electrical recordings of the refolded FhuAΔC/Δ4L (rFhuAΔC/Δ4L) protein.** *A,* circular dichroism spectrum of the rFhuAΔC/Δ4L protein in DDM. 3.42 μM rFhuAΔC/Δ4L protein (see under "Experimental Procedures") was dialyzed against 5 mM Tris, pH 8.32, 100 mM NaCl, and 0.25% (w/v) DDM, and the measurements were carried out at 20 °C. *B,* step increase of the electrical current showing a single-channel insertion of the rFhuAΔC/Δ4L into the lipid bilayer. The rFhuAΔC/Δ4L protein was added to the *cis* side. The transmembrane potential was +20 mV. The increase of current gives a conductance of ~5 nS. *C,* single-channel electrical trace of rFhuAΔC/Δ4L at an applied potential of +40 mV. The expanded trace illustrates the signature of the channel at a greater time resolution. *D,* histogram of the probability (*P*(*G*)) of the occurrence of a given single-channel conductance of rFhuAΔC/Δ4L. *E,* current-voltage relationship of a single rFhuAΔC/Δ4L protein pore. The standard *error bars* were calculated from at least three separate single-channel experiments. Single-channel electrical recordings were acquired in 1 M KCl, 10 mM potassium phosphate, pH 7.4. The single-channel electrical traces were low pass Bessel-filtered at 2 kHz.

the refolded protein retains the overall content of β structure, it cannot determine whether the protein forms a hollow β barrel.

We wanted to inspect whether the rFhuAΔC/Δ4L protein forms an open and stable channel that is closely similar to the mFhuAΔC/Δ4L protein. Indeed, the rFhuAΔC/Δ4L protein readily inserted in the lipid bilayer, as indicated by a discrete stepwise increase of ~100 pA in the current at an applied transmembrane potential of +20 mV (Fig. 5*B*). Similar to the mFhuAΔC/Δ4L protein, rFhuAΔC/Δ4L exhibited irresolvable and rare current spikes (Fig. 5*C* and *expanded trace*). The single-channel conductance of the rFhuAΔC/Δ4L protein was comparable with that of the mFhuAΔC/Δ4L protein pore (4.9 ± 0.7 nS, $n = 25$) at an applied transmembrane potential of +40 mV (Table 3). In contrast to mFhuAΔC/Δ4L, the rFhuAΔC/Δ4L protein pore did not show a broad spectrum of single-channel conductance values (Figs. 4*C* and 5*D*). Finally, we also measured the conductance of the rFhuAΔC/Δ4L protein pore using the I/V curve. The rFhuAΔC/Δ4L protein pore showed an I/V curve that was closely similar to that measured with the mFhuAΔC/Δ4L protein pore (Fig. 5*E*). The single-

channel conductance was ~5.4 nS, which is in accord with the measurement performed at an applied transmembrane potential of +40 mV (Table 3). As in case of mFhuAΔC/Δ4L, 68% of channels conductance values fall within the standard error of the average single-channel conductance (Fig. 5*D*).

DISCUSSION

One major goal of bionanotechnology is to identify protein scaffolds from nature that can be engineered for obtaining robust, versatile, and tractable bionanostructures, which need to be integrated into nanofluidic devices. A particular example is obtaining reliable protein nanopores for single-molecule stochastic sensing of proteins (2, 7) and nucleic acids (55). We explored FhuA, a monomeric 22-stranded β-barrel outer membrane protein of *E. coli*. To obtain insights into the molecular details of different key domains for the development of an open pore, we employed extensive protein design along with electrophysiology. The comparison of the single-channel electrical recordings of the wild-type and mutant FhuA proteins paved the way for us to pinpoint the role of various domains in occluding the β barrel.

In this work, single-channel electrical recordings performed with the WT-FhuA protein revealed that the native channel is not fully closed (~300 pS in 1 M KCl). This result is consistent with prior single-channel electrical data obtained by Braun and co-workers (36, 37), who observed that the WT-FhuA unitary conductance is ~100 pS or less in 1 M KCl. First, what is the reason for obtaining a non-zero current with an outer membrane protein, which is supposed to be closed under equilibrium conditions? Second, what is the cause of some distinction between the single-channel conductance observed in this work and that value previously recorded by Braun and co-workers (36, 37)? Some small ionic flow might be produced by a certain dissociation of the cork domain through the contacts made with the pore walls. There are 60 hydrogen bonds and 9 salt bridges observed in the crystal structure of the WT-FhuA protein (20, 56). Overall, these weak electrostatic interactions make a strong intramolecular contact between the cork domain and the pore walls. It should be noted that under native conditions the transmembrane potential across the outer membrane of Gram-negative bacteria is very small, in which case the cork domain might be tightly connected to the pore walls, contributing to a fully closed channel. It is not clear whether a greater transmembrane potential might dissociate or produce a rearrangement of the cork domain within the pore interior, leading to the passage of ionic flow. Furthermore, the protocols for extraction and purification of the WT-FhuA protein from this work and prior studies are different, which might determine small alterations in the functional features of the reconstituted proteins. In this study, the single channel results with the low conductance WT-FhuA protein channel demonstrate that the large conductance mFhuAΔC/Δ4L and rFhuAΔC/Δ4L protein channels are not produced by contaminating proteins present in various expressing compartments of the cell.

We found that the FhuAΔ1–160 protein pore exhibits a signature decorated by a highly dynamic behavior, featuring current fluctuations between a large conductance (~2.5 nS), open sub-state, S_2, and a low conductance (~0.2 nS), partly closed sub-state, S_1 (Fig. 2*B*). This finding indicates that there is an abrupt alteration of the ion flow across the cork-free FhuA protein channel. Similar results were found with the plug-free mutant of the PapC usher protein channel (57), a 24-stranded β-barrel membrane protein. We rule out that these transitions are caused from the collapse of the β barrel due to the lacking support of the cork, because they were never observed with the engineered FhuAΔC/Δ4L protein pore (Figs. 4 and 5).

We observed that the fluctuations between the S_1 and S_2 sub-states of the cork-free FhuAΔ1–160 protein had a current amplitude of ~ 2.3 nS (Fig. 2*B*). However, the cork-containing FhuAΔ335–355 protein pore exhibited frequent current fluctuations of ~1 nS (Fig. 2*C*). In addition, the cork-free FhuAΔ1–160/Δ335–355 protein pore showed current fluctuations between S_3 and S_2 sub-states of ~1 nS (Fig. 3*B*). These experimental findings suggest that loop L4 is involved in the gating dynamics of the cork-free FhuAΔ1–160 protein channel. This hypothesis is also supported by the structural observations that this loop has a capping role in keeping the cork domain within the pore lumen (20, 21). Furthermore, *in vivo* experiments have shown that the shortening of loop L4 converts the FhuA protein into a passive diffusion channel for ferrichrome (39).

Some questions in our work still remain unanswered, so more molecular engineering and experimentation are needed to address them. One puzzling aspect of our electrical recordings is that the most probable single-channel conductance of the single deletion mutant FhuAΔ335–355 (3.1 ± 0.2 nS, $n = 3$) is closely similar to the unitary conductance of the double deletion mutant FhuAΔ1–160/Δ335–355 (3.0 ± 0.5 nS, $n = 3$) (Table 3). One immediate tentative interpretation is that by deleting various domains, including the cork and extracellular loops, the FhuA protein undergoes a rearrangement of the unmodified loops, altering the overall cross-sectional area of the engineered pore. This is also consistent with some difference in the observed single-channel conductance between the cork-containing FhuAΔ322–355 and FhuAΔ335–355 mutants (Fig. 2*C* and supplemental Fig. S5*B*), but there is a lack of distinction in average single-channel conductance between those values corresponding to the cork-free FhuAΔ1–160/Δ322–355 and FhuAΔ1–160/Δ335–355 proteins (Table 3).

By the systematic deletion of additional long and flexible extracellular loops (L3, L5, and L11; Table 2), we were able to obtain an open and stable protein channel, which is characterized by the largest single-channel conductance (~4.9 nS) ever measured with an engineered FhuA protein (29, 36–39). Remarkably, our electrical recordings with mFhuAΔC/Δ4L and rFhuAΔC/Δ4L have revealed closely similar average unitary conductance values (Figs. 4, *A* and *B*, and 5, *B* and *C*). However, the mFhuAΔC/Δ4L proteins exhibited a broader distribution in single-channel conductance (Figs. 4*C* and 5*D*). It is not clear why the rFhuAΔC/Δ4L protein exhibits a slightly distinct single-channel electrical signature from mFhuAΔC/Δ4L protein. One straightforward explanation is that the two different extraction and purification protocols force the polypeptide chain to obey to dissimilar energetic pathways, the end points of which might be fairly dissimilar. A methodical approach for balancing the experimental conditions pertinent to the refold-

ing of the FhuAΔC/Δ4L protein is now underway in this laboratory.

It should be noted that this work does not indicate which way the engineered FhuA proteins insert into the lipid bilayer. When mFhuAΔC/Δ4L is added to the *cis* chamber, it produces channels that insert in only one direction. This argument is based upon the current-voltage relationship of this engineered FhuA protein pore. For example, we noticed single-channel currents of approximately +220 and approximately −232 pA at a transmembrane potential of +40 and −40 mV, respectively (Fig. 4*D*). One way to tackle this issue concerning the orientation of the FhuAΔC/Δ4L protein is to attach a small ligand in the proximity of one entrance of the channel and a binding protein added to one of the chambers. The ligand-binding protein interaction could be observed either by single-channel or macroscopic current measurements, indicating the insertion direction of the FhuAΔC/Δ4L protein.

In a recent paper, Udho *et al.* (58) hypothesized that 4 M urea facing the periplasmic side of the WT-FhuA protein initiates the unfolding of the cork domain, opening an ion-conducting pathway through the native protein. Because all their experiments were performed with the WT-FhuA protein, it is not clear whether a rearrangement of the cork domain within the pore interior due to the presence of urea in the periplasmic side is accompanied by conformational alterations of the long extracellular loops (L3, L4, L5, and L11; Table 2). Our experiments presented in this paper (Fig. 2, *B* and *C*) and also previous electrophysiology studies with other deletion mutants of the FhuA protein (36–38) clearly indicated measurable single-channel and macroscopic ion currents with engineered cork-containing FhuA protein channels. Interestingly, Udho *et al.* (58) found that a 3 M glycerol-induced osmotic gradient can help the insertion of the WT-FhuA protein into the planar lipid membrane but in both orientations. Therefore, it was concluded that 4 M urea within the chamber played a dual role as follows: (i) it unfolded the cork domain, and (ii) it produced an osmotic gradient across the membrane required for the protein insertion. These results are quite distinct from what we have learned, for example, with trimeric outer membrane porins, which insert directly into the membrane with the extracellular side facing the *cis* chamber and with the periplasmic side oriented toward the *trans* chamber. Moreover, their findings contrast this work with the engineered FhuAΔC/Δ4L protein pore, which inserts spontaneously into the membrane in a single orientation and in the absence of any osmotic gradient.

A different approach to open the WT-FhuA protein channel is to use phage T5. Bonhivers *et al.* (29) showed binding activity of the T5 phage to the WT-FhuA protein, producing large conductance stepwise discrete changes in the macroscopic current. Undoubtedly, an open and highly stable monomeric β-barrel pore with a wide diameter would be desirable in many biosensing applications. Potential use of this approach is the design of stochastic sensing elements for dsDNA (59), polypeptides (60–63), and their ensembles. For example, such a protein nanopore would accommodate folded protein domains and dsDNA, which is not achievable with the trimeric OmpF, heptameric αHL, or even with the monomeric OmpG protein pores due to their constricted diameters of ~15 Å. However, the x-ray crystal structure of the FhuA protein shows a large cluster of negatively charged residues throughout the β-barrel pore walls and β turns (20, 21), indicating the cation selectivity of the engineered FhuA protein channel, in accord with prior electrophysiological determinations (29, 39). A large pool of negative charges within the interior of the engineered FhuAΔC/Δ4L protein pore generates a high energetic barrier for passing negatively charged dsDNA from one side of the chamber to the other. Therefore, such single-molecule translocation experiments might be successful, if a number of negative charges of the pore lumen will be neutralized by their replacement with other uncharged residues. Alternatively, the engineering of positive side chains within the interior of the pore might catalyze the capture rate and translocation of the dsDNA across the FhuAΔC/Δ4L protein pore (61, 64).

Recently, Wendell *et al.* (59) explored the translocation of dsDNA through a membrane-adapted ϕ29 motor protein nanopore. The internal diameter of this nanopore varies between 3.6 and 6.0 nm, whereas the height is 7.0 nm. Interestingly, the single-channel conductance of the membrane-adapted ϕ29 motor protein nanopore was 4.8 nS in 1 M KCl, which is identical to the average single-channel conductance measured with FhuAΔC/Δ4L. The cross-sectional sides of the engineered FhuAΔC/Δ4L protein pore are 3.1 and 4.4 nm, whereas the smallest and largest heights are 2.9 and 6.2 nm, respectively. Notably, the connector protein of the ϕ29 nanopore consists of 12 GP10 protein subunits. This dodecamer stoichiometry limits the versatility of the ϕ29 motor protein nanopore to further molecular engineering of individual pore subunits.

In summary, we have successfully engineered a monomeric β-barrel protein, which forms large conductance and stable single channels in planar lipid bilayer, as judged by high resolution electrical recordings. We showed that it is possible to radically redesign an outer membrane protein with a highly distinct functionality from the native protein. This newly redesigned monomeric protein can be easily altered by engineering targeted functional groups at strategic positions within the interior of the pore. Therefore, FhuA serves as a versatile model for exploring the folding and stability of integral membrane proteins and their relationship to the mechanisms of gating dynamics and ion conductance. The WT-FhuA protein is meant to keep the passage of small molecules from occurring, except under specific energy-dependent conditions (27). In contrast, the large conductance FhuAΔC/Δ4L protein channel, with the cross-sectional sides of 3.1 × 4.4 nm, is conceivably "translocation-competent" for bulky biopolymers. Certainly, the FhuAΔC/Δ4L protein pore might serve as a natural scaffold for the design and development of nanopore-based sensing elements. For example, electrostatic and hydrophobic groups can be engineered at desired positions within the pore lumen with atomic precision. From a technical point of view, we also showed that by utilizing two distinct extraction and purification procedures, detergent-assisted membrane extraction and refolding from inclusion bodies, we were able to obtain an engineered FhuAΔC/Δ4L protein with a closely similar large single-channel conductance but a slightly different electrical signature. Moreover, customized and redesigned FhuA proteins

with well defined biophysical, biochemical, and structural features might also be used in gene delivery, drug loading, and encapsulation techniques for medical biotechnology (41, 65, 66).

Acknowledgments—We thank Ulrich Schwaneberg for the gift of WT FhuA and FhuAΔ1–160 plasmids. We are also grateful to Helge Weingart for gifting the E. coli expression host. We thank Stewart Loh for help in obtaining the circular dichroism measurements and Phillip K. Borer, Deborah Kerwood, and Damian Allis for their assistance in constructing and running the molecular dynamics simulations.

REFERENCES

1. Bayley, H., and Cremer, P. S. (2001) *Nature* **413,** 226–230
2. Movileanu, L. (2009) *Trends Biotechnol.* **27,** 333–341
3. Howorka, S., and Siwy, Z. (2009) *Chem. Soc. Rev.* **38,** 2360–2384
4. Song, L., Hobaugh, M. R., Shustak, C., Cheley, S., Bayley, H., and Gouaux, J. E. (1996) *Science* **274,** 1859–1866
5. van den Berg, B. (2005) *Curr. Opin. Struct. Biol.* **15,** 401–407
6. Bayley, H., Braha, O., Cheley, S., and Gu, L. Q. (2004) in *NanoBiotechnology* (Niemeyer, C. M., and Mirkin, C. A., eds) pp. 93–112, Wiley-VCH Verlag GmbH & Co. KGaA, Weinheim, Germany
7. Movileanu, L. (2008) *Soft Matter* **4,** 925–931
8. Nestorovich, E. M., Danelon, C., Winterhalter, M., and Bezrukov, S. M. (2002) *Proc. Natl. Acad. Sci. U.S.A.* **99,** 9789–9794
9. Berkane, E., Orlik, F., Charbit, A., Danelon, C., Fournier, D., Benz, R., and Winterhalter, M. (2005) *J. Nanobiotechnology* **3,** 3
10. Chimerel, C., Movileanu, L., Pezeshki, S., Winterhalter, M., and Kleinekathöfer, U. (2008) *Eur. Biophys. J.* **38,** 121–125
11. Howorka, S., Movileanu, L., Lu, X. F., Magnon, M., Cheley, S., Braha, O., and Bayley, H. (2000) *J. Am. Chem. Soc.* **122,** 2411–2416
12. Bikwemu, R., Wolfe, A. J., Xing, X., and Movileanu, L. (2010) *J. Phys. Condens. Matter* **22,** 454117
13. Movileanu, L., Howorka, S., Braha, O., and Bayley, H. (2000) *Nat. Biotechnol.* **18,** 1091–1095
14. Jung, Y., Bayley, H., and Movileanu, L. (2006) *J. Am. Chem. Soc.* **128,** 15332–15340
15. Subbarao, G. V., and van den Berg, B. (2006) *J. Mol. Biol.* **360,** 750–759
16. Chen, M., Khalid, S., Sansom, M. S., and Bayley, H. (2008) *Proc. Natl. Acad. Sci. U.S.A.* **105,** 6272–6277
17. Mohammad, M. M., Prakash, S., Matouschek, A., and Movileanu, L. (2008) *J. Am. Chem. Soc.* **130,** 4081–4088
18. Mohammad, M. M., and Movileanu, L. (2008) *Eur. Biophys. J.* **37,** 913–925
19. Kasianowicz, J. J., Brandin, E., Branton, D., and Deamer, D. W. (1996) *Proc. Natl. Acad. Sci. U.S.A.* **93,** 13770–13773
20. Locher, K. P., Rees, B., Koebnik, R., Mitschler, A., Moulinier, L., Rosenbusch, J. P., and Moras, D. (1998) *Cell* **95,** 771–778
21. Ferguson, A. D., Hofmann, E., Coulton, J. W., Diederichs, K., and Welte, W. (1998) *Science* **282,** 2215–2220
22. Bonhivers, M., Desmadril, M., Moeck, G. S., Boulanger, P., Colomer-Pallas, A., and Letellier, L. (2001) *Biochemistry* **40,** 2606–2613
23. Ramakrishnan, M., Pocanschi, C. L., Kleinschmidt, J. H., and Marsh, D. (2004) *Biochemistry* **43,** 11630–11636
24. Ramakrishnan, M., Qu, J., Pocanschi, C. L., Kleinschmidt, J. H., and Marsh, D. (2005) *Biochemistry* **44,** 3515–3523
25. Pawelek, P. D., Croteau, N., Ng-Thow-Hing, C., Khursigara, C. M., Moiseeva, N., Allaire, M., and Coulton, J. W. (2006) *Science* **312,** 1399–1402
26. Ferguson, A. D., Ködding, J., Walker, G., Bös, C., Coulton, J. W., Diederichs, K., Braun, V., and Welte, W. (2001) *Structure* **9,** 707–716
27. Braun, V. (2009) *J. Bacteriol.* **191,** 3431–3436
28. Destoumieux-Garzón, D., Duquesne, S., Peduzzi, J., Goulard, C., Desmadril, M., Letellier, L., Rebuffat, S., and Boulanger, P. (2005) *Biochem. J.* **389,** 869–876
29. Bonhivers, M., Ghazi, A., Boulanger, P., and Letellier, L. (1996) *EMBO J.* **15,** 1850–1856
30. Letellier, L., Plançon, L., Bonhivers, M., and Boulanger, P. (1999) *Res. Microbiol.* **150,** 499–505
31. Lambert, O., Letellier, L., Gelbart, W. M., and Rigaud, J. L. (2000) *Proc. Natl. Acad. Sci. U.S.A.* **97,** 7248–7253
32. Böhm, J., Lambert, O., Frangakis, A. S., Letellier, L., Baumeister, W., and Rigaud, J. L. (2001) *Curr. Biol.* **11,** 1168–1175
33. Mdzinarashvili, T., Khvedelidze, M., Ivanova, A., Mrevlishvili, G., Kutateladze, M., Balarjishvili, N., Celia, H., and Pattus, F. (2006) *Eur. Biophys. J.* **35,** 231–238
34. Cao, Z., and Klebba, P. E. (2002) *Biochimie* **84,** 399–412
35. Faraldo-Gómez, J. D., Smith, G. R., and Sansom, M. S. (2003) *Biophys. J.* **85,** 1406–1420
36. Killmann, H., Benz, R., and Braun, V. (1993) *EMBO J.* **12,** 3007–3016
37. Braun, V., Killmann, H., and Benz, R. (1994) *FEBS Lett.* **346,** 59–64
38. Killmann, H., Benz, R., and Braun, V. (1996) *J. Bacteriol.* **178,** 6913–6920
39. Braun, M., Killmann, H., Maier, E., Benz, R., and Braun, V. (2002) *Eur. J. Biochem.* **269,** 4948–4959
40. Endriss, F., and Braun, V. (2004) *J. Bacteriol.* **186,** 4818–4823
41. Nallani, M., Benito, S., Onaca, O., Graff, A., Lindemann, M., Winterhalter, M., Meier, W., and Schwaneberg, U. (2006) *J. Biotechnol.* **123,** 50–59
42. Hoffmann, H., Fischer, E., Kraut, H., and Braun, V. (1986) *J. Bacteriol.* **166,** 404–411
43. Chow, M. K., Amin, A. A., Fulton, K. F., Fernando, T., Kamau, L., Batty, C., Louca, M., Ho, S., Whisstock, J. C., Bottomley, S. P., and Buckle, A. M. (2006) *Nucleic Acids Res.* **34,** D207–D212
44. Movileanu, L., Neagoe, I., and Flonta, M. L. (2000) *Int. J. Pharm.* **205,** 135–146
45. Movileanu, L., and Bayley, H. (2001) *Proc. Natl. Acad. Sci. U.S.A.* **98,** 10137–10141
46. Movileanu, L., Cheley, S., Howorka, S., Braha, O., and Bayley, H. (2001) *J. Gen. Physiol.* **117,** 239–252
47. Movileanu, L., Cheley, S., and Bayley, H. (2003) *Biophys. J.* **85,** 897–910
48. Movileanu, L., Schmittschmitt, J. P., Scholtz, J. M., and Bayley, H. (2005) *Biophys. J.* **89,** 1030–1045
49. Dundas, J., Ouyang, Z., Tseng, J., Binkowski, A., Turpaz, Y., and Liang, J. (2006) *Nucleic Acids Res.* **34,** W116–W118
50. Mohammad, M. M., and Movileanu, L. (2010) *J. Phys. Chem. B* **114,** 8750–8759
51. Boulanger, P., le Maire, M., Bonhivers, M., Dubois, S., Desmadril, M., and Letellier, L. (1996) *Biochemistry* **35,** 14216–14224
52. Whitmore, L., and Wallace, B. A. (2008) *Biopolymers* **89,** 392–400
53. Whitmore, L., and Wallace, B. A. (2004) *Nucleic Acids Res.* **32,** W668–W673
54. Provencher, S. W., and Glöckner, J. (1981) *Biochemistry* **20,** 33–37
55. Branton, D., Deamer, D. W., Marziali, A., Bayley, H., Benner, S. A., Butler, T., Di Ventra, M., Garaj, S., Hibbs, A., Huang, X., Jovanovich, S. B., Krstic, P. S., Lindsay, S., Ling, X. S., Mastrangelo, C. H., Meller, A., Oliver, J. S., Pershin, Y. V., Ramsey, J. M., Riehn, R., Soni, G. V., Tabard-Cossa, V., Wanunu, M., Wiggin, M., and Schloss, J. A. (2008) *Nat. Biotechnol.* **26,** 1146–1153
56. Endriss, F., Braun, M., Killmann, H., and Braun, V. (2003) *J. Bacteriol.* **185,** 4683–4692
57. Mapingire, O. S., Henderson, N. S., Duret, G., Thanassi, D. G., and Delcour, A. H. (2009) *J. Biol. Chem.* **284,** 36324–36333
58. Udho, E., Jakes, K. S., Buchanan, S. K., James, K. J., Jiang, X., Klebba, P. E., and Finkelstein, A. (2009) *Proc. Natl. Acad. Sci. U.S.A.* **106,** 21990–21995
59. Wendell, D., Jing, P., Geng, J., Subramaniam, V., Lee, T. J., Montemagno, C., and Guo, P. (2009) *Nat. Nanotechnol.* **4,** 765–772
60. Goodrich, C. P., Kirmizialtin, S., Huyghues-Despointes, B. M., Zhu, A., Scholtz, J. M., Makarov, D. E., and Movileanu, L. (2007) *J. Phys. Chem. B* **111,** 3332–3335
61. Wolfe, A. J., Mohammad, M. M., Cheley, S., Bayley, H., and Movileanu, L. (2007) *J. Am. Chem. Soc.* **129,** 14034–14041
62. Talaga, D. S., and Li, J. (2009) *J. Am. Chem. Soc.* **131,** 9287–9297
63. Niedzwiecki, D. J., Grazul, J., and Movileanu, L. (2010) *J. Am. Chem. Soc.* **132,** 10816–10822
64. Maglia, G., Restrepo, M. R., Mikhailova, E., and Bayley, H. (2008) *Proc.*

Natl. Acad. Sci. U.S.A. **105,** 19720–19725
65. Nallani, M., Onaca, O., Gera, N., Hildenbrand, K., Hoheisel, W., and Schwaneberg, U. (2006) *Biotechnol. J.* **1,** 828–834
66. Onaca, O., Sarkar, P., Roccatano, D., Friedrich, T., Hauer, B., Grzelakowski, M., Güven, A., Fioroni, M., and Schwaneberg, U. (2008) *Angew. Chem. Int. Ed. Engl.* **47,** 7029–7031
67. Biswas, S., Mohammad, M. M., Patel, D. R., Movileanu, L., and van den Berg, B. (2007) *Nat. Struct. Mol. Biol.* **14,** 1108–1109
68. Biswas, S., Mohammad, M. M., Movileanu, L., and van den Berg, B. (2008) *Structure* **16,** 1027–1035
69. Schirmer, T., Keller, T. A., Wang, Y. F., and Rosenbusch, J. P. (1995) *Science* **267,** 512–514
70. Arora, A., Rinehart, D., Szabo, G., and Tamm, L. K. (2000) *J. Biol. Chem.* **275,** 1594–1600
71. Cowan, S. W., Garavito, R. M., Jansonius, J. N., Jenkins, J. A., Karlsson, R., König, N., Pai, E. F., Pauptit, R. A., Rizkallah, P. J., and Rosenbusch, J. P. (1995) *Structure* **3,** 1041–1050
72. Ferguson, A. D., Chakraborty, R., Smith, B. S., Esser, L., van der Helm, D., and Deisenhofer, J. (2002) *Science* **295,** 1715–1719
73. Buchanan, S. K., Smith, B. S., Venkatramani, L., Xia, D., Esser, L., Palnitkar, M., Chakraborty, R., van der Helm, D., and Deisenhofer, J. (1999) *Nat. Struct. Biol.* **6,** 56–63
74. Chimento, D. P., Mohanty, A. K., Kadner, R. J., and Wiener, M. C. (2003) *Nat. Struct. Biol.* **10,** 394–401
75. Cherezov, V., Yamashita, E., Liu, W., Zhalnina, M., Cramer, W. A., and Caffrey, M. (2006) *J. Mol. Biol.* **364,** 716–734
76. Huang, Y., Smith, B. S., Chen, L. X., Baxter, R. H., and Deisenhofer, J. (2009) *Proc. Natl. Acad. Sci. U.S.A.* **106,** 7403–7407